A One-Dimensional Model for Polymer Melting During Modulated Temperature Differential Scanning Calorimetry

A. A. Lacey * C. V. Nikolopoulos †

Abstract

A one-dimensional model for the melting of polymers, assuming the polymer crystals take the form of lamellæ, or thin sheets of material, is discussed. The model is derived on the assumption that the melting point of a lamella depends upon its thickness, that a lamella melts the instant this temperature is exceeded, and that lamellæ with higher melting points grow by accumulating surplus of melt. The model is analyzed for a temperature control that is the sum of a linear and a sinusoidal function of time as in Modulated Temperature Differential Scanning Calorimetry (MTDSC), which is a technique for measuring thermal properties of materials. This work is an extension of a previous paper, by the same authors, considering a homogeneous model, based on the same assumptions. Some predictions regarding the output of such calorimetry are made.

Keywords. Modulated temperature differential scanning calorimetry, polymer melting, perturbation methods.

1 Introduction

Modulated temperature differential scanning calorimetry or MTDSC is a method introduced by Reading and collaborators for measuring the thermal properties of materials [4], [5], [6], [7]. In this method, conventional DSC is used with the modification that the usual programme of linearly increasing temperature is modulated by a periodic perturbation.

During an experiment, a sample of the material under investigation is placed in one of two pans, the other of which is empty but otherwise identical, and these pans are positioned symmetrically within the calorimeter. Heat is supplied to (or removed from) the calorimeter in a controlled and (spatially) symmetric way so that the sample's temperature follows a preset programme. The temperature difference between the sample and the reference pan is monitored. This gives a measure of the rate of heat intake (or output) by the sample and allows quantities such as the heat capacity to be determined. More precisely, the calorimeter, or "furnace", is heated so that the temperature rise is linear with an addition of sinusoidal modulation (controlled in such a way so that the sample's temperature has the required form) and the response, *i.e.*, the release or absorption of heat due to temperature variation, of the sample is measured; such a heat flow is determined by the temperature difference between the two pans. Measuring the temperature difference between the two pans enables one to find the response of the sample purely to the preset temperature programme. Then the sample's thermal properties can be deduced.

This measure of heat transfer is split into a slowly varying part, the "underlying signal," and an oscillatory part (or at least its first harmonic), the "cyclic signal". These two signals can both be determined in an experiment.

MTDSC measurements can be used to deduce both qualitative and quantitative information about the sample's nature, *e.g.*, its consistency, specific heat, latent heat, the general behaviour of the sample under a transition, *etc.* Also it is useful for thermal characterization of the sample, since the sample's thermal response can be compared with already existing data. There is now a need for further theoretical analysis of MTDSC operation in order to optimize interpretation of the measurements.

In standard MTDSC, heating/cooling is done sinusoidally. Provided that the amplitude is small enough, the sample behaves linearly. This means that any quantity $g(T_s)$, depending on sample temperature

$$T_s = bt + B\sin\omega t\,, \tag{1}$$

can be linearized and written as $g(T_s) = g(bt) + Bg'(bt)\sin\omega t$. There will also be sinusoidal heat intake/output, and all temperatures can be thought of as consisting of an underlying and a cyclic part, the latter having negligible higher harmonics.

* School of Mathematical and Computer Sciences, Heriot-Watt University, Riccarton, Edinburgh, EH14 4AS, UK (A.A.Lacey@ma.hw.ac.uk).
† Department of Mathematics, University of Aegean, Karlovasi, Samos, Greece (cnikolo@aegean.gr).

Both the underlying and cyclic parts of the temperature are generated by controlling the heat supply. The amplitude B can be increased/reduced by varying the amplitude of the changes in heating. There will, in general, be a phase difference between the heat supply and the temperature of the sample, and this phase will normally vary during the course of an experiment. The actual phase of the temperature, relative to the forcing, is not particularly important for an analysis of the results, and we shall generally simply take the sample temperature oscillations to be $B\sin(\omega t)$.

The simplest model for the calorimeter (see [2]) is given by neglecting its internal heat capacity, and, without loss of generality, a pair of ordinary differential equations represents the heat flows into the pans with their associated changes of temperature:

$$\frac{\mathrm{d}Q_s}{\mathrm{d}t} = (C_r + C_s)\frac{\mathrm{d}T_s}{\mathrm{d}t} + g = K_1(T_r - T_s) + K_0(T_f - T_s)\,, \tag{2}$$

$$\frac{\mathrm{d}Q_r}{\mathrm{d}t} = C_r\frac{\mathrm{d}T_r}{\mathrm{d}t} = K_1(T_s - T_r) + K_0(T_f - T_r)\,. \tag{3}$$

Here K_0 is the heat-transfer coefficient between the pans and the exterior of the calorimeter while K_1 is that between the pans, C_r is the heat capacity of each pan, C_s is the heat capacity of the actual sample, and g is the rate of heat absorption by the sample by any chemical reaction, phase transition, *etc.*

The temperature of the furnace T_f can be eliminated, simply, making use of symmetry (see [2]). The temperature difference between the reference and the sample, $\Delta T = (T_r - T_s)$, then satisfies the equation

$$C_r\frac{\mathrm{d}\Delta T}{\mathrm{d}t} + K\Delta T = C_s\frac{\mathrm{d}T_s}{\mathrm{d}t} + g\,,$$

with $K = 2K_1 + K_0$. For B small enough to allow linearization we have $\Delta T = \Delta\overline{T} + \Delta\widetilde{T}$ and $g = \bar{g} + \tilde{g} = \bar{g} + \mathrm{Re}\,\{\hat{g}\exp \mathrm{i}\omega t\}$ so that

$$\Delta\overline{T} = \frac{1}{K}(C_s b + \bar{g})\,,$$

assuming that transients can be neglected, while

$$\Delta\widetilde{T} = B\omega\mathrm{Re}\left\{\frac{C_s + \mathrm{i}\hat{g}/B\omega}{K + \mathrm{i}\omega C_r}\,e^{\mathrm{i}\omega t}\right\}.$$

During an MTDSC run $\Delta\overline{T}$ and $\Delta\widetilde{T}$ are measured, and experimental values of the underlying and cyclic heat capacity can be calculated from the formulas $\overline{C} = K\Delta\overline{T}/b$ and $\widetilde{C} = \sqrt{(K^2 + \omega^2 C_R^2)}|\Delta\widetilde{T}|/\omega B$, respectively, where by $|\cdot|$ we denote the amplitude of a quantity; see [1], [2], [6], [8], [9]. (The phase of the cyclic measurement $\widetilde{T}$, *i.e.* the argument of $\widehat{T}$, can be used to obtain a refined estimate of heat capacity.) For an inert sample $g \equiv 0$ in an experiment so we have $\overline{C} = \widetilde{C} = C_s$. Using the above expressions for $\Delta\overline{T}$ and $\Delta\widetilde{T}$, we have, more generally, that the underlying and cyclic measurements of heat capacity, $\overline{C}$ and $\widetilde{C}$, respectively, will be related to g by the following formulas:

$$\overline{C} = C_s + \bar{g}/b, \tag{4}$$

$$\widetilde{C} = |C_s + \hat{g}/\omega B|. \tag{5}$$

The main problem studied in this work is the modelling of the melting process inside a polymer sample. It is assumed that the polymer crystals take the form of lamellæ or thin sheets of material. In this way we can determine the heat absorption g, and consequently $\bar{g}$ and $\hat{g}$, for this specific process. It is then possible to use the ODE model, presented above, for the calorimeter as a whole, to simulate the MTDSC signal for such a sample, using (4) and (5) to predict the underlying and cyclic measurements, or "signals".

The earlier paper, [3], developed an ODE model, based on treating the sample as a spatially uniform object. The predictions of that model were generally in good agreement with experiment, except that, with an assumption of perfect control of the sample's temperature and for small amplitudes of oscillation, the cyclic signal (measurement of the heat capacity) was never below the underlying one. In practice, although the cyclic signal is the larger of the two in the early stages of melting, the two signals cross and the underlying one is the larger at higher temperatures. For other processes which can occur in samples, such as chemical reactions, the associated time scale, or "kinetic effect", tends to reduce the cyclic measurment relative to the underlying one. In a sample with non-zero size the finite thermal conductivity can introduce a similar kinetic effect. This would allow the possibility, even with ideal control of the sample's surface temperature, of the crossing of the two signals. This key influence of finite thermal conductivity is investigated in the present work.

We start, in the following section, by summarising the model for polymer melting. In Section 3, some of the results of [3] which are important for this paper are reviewed, the full dimensionless model, which couples polymer melting with heat transfer, is simplified and important parameter regimes are identified. The consequences of these, in cases which can be treated analytically, are discussed in Section 4. Even the simplified models cannot be solved fully for all time so some numerical simulations and results are presented in Section 5.

2 The Lamella Model

The polymer sample is taken to consist of a crystalline, low-temperature, phase, made up of thin sheets, or lamellæ, and an amorphous phase, the "melt". The melting point of a particular lamella is governed by its thickness and we can regard each lamella as being characterised by its melting temperature, T_m, and size, say its mass or the total length of polymer chain within it, s. The time scale of an experiment is assumed to be short enough for nucleation to be neglected. This means that once the temperature T at some point x within the sample has exceeded a given T_m there will subsequently be no lamellæ corresponding to T_m at x. Before such a time the density function $\mathcal{D}$ for the distribution of lamellæ is positive. This density function is defined by:

number of lamellæ lying in a volume $\mathrm{d}V$ near a point x, with melting temperature between T_m and $T_m + \mathrm{d}T_m$ and size between s and $s + \mathrm{d}s$ is $\mathcal{D}(x, t, s, T_m)\,\mathrm{d}V\,\mathrm{d}T_m\,\mathrm{d}s$.

The number density with respect to x and T_m is then

$$\mathcal{N}(x, t, T_m) = \int_0^\infty \mathcal{D}(x, t, s, T_m)\,\mathrm{d}s\,.$$

For simplicity we suppose that the sample is initially homogeneous, so $\mathcal{D}(x, 0, s, T_m)$ is independent of x, and that $\mathcal{D}$ is scaled so that $\mathcal{N}(x, 0, T_m) \equiv \mathcal{N}^*(T_m)$ satisfies

$$\int_0^\infty \mathcal{N}^*(T_m)\,\mathrm{d}T_m = 1\,.$$

A related density is the mass density with respect to T_m at position x and time t:

$$\mathcal{M}(x, t, T_m) = \int_0^\infty \mathcal{D}(x, t, s, T_m)\, s\,\mathrm{d}s\,,$$

with s scaled appropriately. Another assumption, which is simply made for convenience, is that there is no amorphous polymer if the sample is in equilibrium and there are some lamellæ present. (The minimum melt fraction might instead be some positive value α^*, dependent perhaps upon crystal size distribution. This was seen in [3] not to affect the qualitative behaviour of the model greatly.) In particular, at the start of an experiment,

$$\mathcal{M}(x, 0, T_m) \equiv \mathcal{M}^*(T_m) \text{ satisfies } \int_0^\infty \mathcal{M}^*(T_m)\,\mathrm{d}T_m = \rho = \text{ total polymer density.}$$

For subsequent times, there can be some melt present so for $t > 0$, $\int_0^\infty \mathcal{M}(x, t, T_m)\,\mathrm{d}T_m \le 1$ and

$$\alpha(x, t) = \text{local mass fraction for the melt} = 1 - \frac{1}{\rho}\int_0^\infty \mathcal{M}(x, t, T_m)\,\mathrm{d}T_m \ge 0\,.$$

The assumption about negligible nucleation means that

$$\mathcal{N}(x, t, T_m) = 0 \text{ and } \mathcal{M}(x, t, T_m) = 0 \text{ for } T_l(x, t) \equiv \sup_{0<t'<t} T(x, t') > T_m\,.$$

It also implies that

$$\mathcal{N}(x, t, T_m) = \mathcal{N}^*(T_m) \qquad \text{for } T_l(x, t) < T_m\,.$$

All the melt present at any time is here supposed available for recrystallisation onto surviving lamellæ, thereby increasing their size. The growth law governing this process is assumed to be of the form

$$\frac{\partial}{\partial t}\mathcal{M}(x, t, T_m) = F(T)\mathcal{N}(x, t, T_m) \qquad \text{where } T > T_m \text{ and } \alpha > 0\,;$$

more general laws are possible, for instance having the positive function F dependent upon T_m as well as T or allowing the right-hand side to be proportional to some increasing function of α. With $\alpha = 0$ the growth of remaining lamellæ is potentially limited by the rate of melting,

$$\mathcal{M}(x,t,T)\frac{\partial T}{\partial t} = \mathcal{M}(x,t,T)\frac{\partial T_l}{\partial t} = \mathcal{M}(x,t,T_l)\frac{\partial T_l}{\partial t}$$

($T \le T_l$, and, if $T < T_l$, $\partial T_l/\partial t = \mathcal{M}(x,t,T) = 0$) and the rate of take up is again assumed to be determined by number density,

$$\frac{\partial}{\partial t}\mathcal{M}(x,t,T_m) = \mathcal{N}(x,t,T_m) \times \min\left\{F(T), \frac{\mathcal{M}(x,t,T)\partial T/\partial t}{\int \mathcal{N}(x,t,T_m')\,\mathrm{d}T_m'}\right\}.$$

Correspondingly, the rate of change of the melt density is

$$\rho\frac{\partial \alpha}{\partial t} = \begin{cases} \mathcal{M}(x,t,T)\dfrac{\partial T}{\partial t} - F(T)\displaystyle\int \mathcal{N}(x,t,T_m')\,\mathrm{d}T_m' & \text{for } \alpha > 0 \\ \max\left\{0, \mathcal{M}(x,t,T)\dfrac{\partial T}{\partial t} - F(T)\displaystyle\int \mathcal{N}(x,t,T_m')\,\mathrm{d}T_m'\right\} & \text{for } \alpha = 0 \end{cases}.$$

The rate of conversion of polymer from lamellæ to melt is asociated with a rate of take up of latent heat at a rate $L\rho\ \partial\alpha/\partial t$ per unit volume, where L is the latent heat of melting.

Any density variation associated with the change from the crystalline to the amorphous state is neglected in the present work.

3 The Scaled Model and Earlier Results

The sample is typically a thin disc, with half-width ℓ and cross-sectional area A, of the substance under investigation (see Fig. 1). With ℓ sufficiently small compared with the radius of the circular cross-section, it is

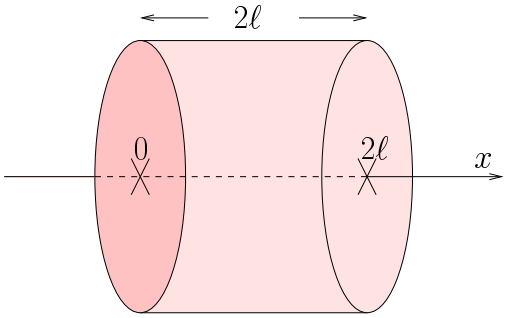

Figure 1: A cylindrical sample of thickness 2ℓ.

appropriate to use a one-dimensional model and to scale x with ℓ: $x = \ell y$.

If the melting occurs in a limited range of temperatures, which is what would usually be observed, say between T_1 and T_2, then we have $\mathcal{N} = 0$ and $\mathcal{M} = 0$ for $T_m < T_1$ and for $T_m > T_2$ and it is reasonable to scale temperature according to

$$T = T_1 + (T_2 - T_1)\theta\,. \tag{6}$$

In MTDSC the sample's temperature would be ideally controlled to be the sum of a linear ramp and a sinusoidal part. In this paper, it is indeed assumed that the device is run with such a temperature on the surface of the sample. More complicated, and realistic, models are of course possible. Associated with (6), and the temperature ramp b, a new time variable can be defined by

$$t = ((T_2 - T_1)\tau + T_1)/b$$

so that $\tau = 0$ at about the start of melting and $\tau = 1$ at about its completion (subject to a slight perturbation resulting from the small sinusoidal part of temperature). The dimensionless temperature at the sample's surface is then

$$\theta_s = \tau + \frac{\lambda}{\Omega}\sin\Omega\tau\,, \tag{7}$$

where λ is the dimensionless amplitude of the rate of change of temperature and is typically order one, while the non-dimensional angular frequency, Ω, is large [3]. With $\Omega \gg 1$, the method of multiple scales can be used,

see below and [3], to analyse the model. Indeed, for the decomposition of signals into underlying and cyclic parts to be viable there must be many oscillations during the course of a transition and Ω of order $100 \gg 1$ is reasonable in practice, [3].

The lamella melting number and mass densities are written as

$$\mathcal{N} = \frac{n}{A\ell(T_2 - T_1)} \qquad \text{and} \qquad \mathcal{M} = \frac{\rho m}{A\ell(T_2 - T_1)}\,.$$

The dimensionless problem becomes

$$\frac{\partial m}{\partial \tau}(y,\tau,\varphi) = \begin{cases} f(\theta)n(\varphi) & \text{if } \alpha > 0 \\ \dfrac{n(\varphi)m(y,\tau,\theta)}{\int_\Theta^\infty n(\phi)\,\mathrm{d}\phi}\dfrac{\partial\theta}{\partial\tau} & \text{if } \alpha = 0 \end{cases} \tag{8}$$

for the lamella melting point φ greater than the largest local temperature so far:

$$\varphi > \Theta(y,\tau) \equiv \sup_{\tau'<\tau}\{\theta(y,\tau')\}\,.$$

Also for $\varphi > \Theta$, $n =$ constant $= n^*$, while $m = n = 0$ for $\varphi < \Theta$. The melt fraction is then given by

$$\frac{\partial \alpha}{\partial \tau}(y,\tau) = \begin{cases} m(y,\tau,\theta)\dfrac{\partial\theta}{\partial\tau} - f(\theta)\displaystyle\int_\Theta^\infty n^*(\phi)\,\mathrm{d}\phi & \text{if } \alpha > 0 \\ \max\left\{0, = 20m(y,\tau,\theta)\dfrac{\partial\theta}{\partial\tau} - f(\theta)\displaystyle\int_\Theta^\infty n^*(\phi)\,\mathrm{d}\phi\right\} & \text{if } \alpha = 0 \end{cases}\,. \tag{9}$$

=46rom the scaling, $\int m\,\mathrm{d}\phi = \int n\,\mathrm{d}\phi = 1$ for sufficiently negative τ. Also note that

$$m(y,\tau,\theta)\frac{\partial\theta}{\partial\tau} = m(y,\tau,\theta)\frac{\partial\Theta}{\partial\tau} = m(y,\tau,\Theta)\frac{\partial\Theta}{\partial\tau}\,.$$

Turning to energy and temperature, and assuming that the density, ρ, specific heat, c, and thermal conductivity, k, are all constant, the dimensionless heat equation is

$$\frac{\partial\theta}{\partial\tau} = D\frac{\partial^2\theta}{\partial y^2} - l\frac{\partial\alpha}{\partial\tau} \qquad \text{for } 0 < y < 1\,, \tag{10}$$

where $l\dfrac{\partial\alpha}{\partial\tau}$ is the dimensionless rate of absorption of heat by melting. The coefficients are a scaled diffusivity, $D = (T_2 - T_1)k/b\ell^2\rho c$, and a scaled latent heat, $l = L/c(T_2 - T_1)$. This equation is subject to the boundary conditions

$$\theta = \tau + \tilde{\lambda}\sin\Omega\tau \qquad \text{on } y = 0\,, \tag{11}$$

$$\frac{\partial\theta}{\partial y} = 0 \qquad \text{on } y = 1\,. \tag{12}$$

The former comes from assuming that the surface temperature is ideally controlled, (7), with dimensionless frequency $\Omega = \omega(T_2 - T_2)/b$ and amplitude $\tilde{\lambda} = \lambda/\Omega = B/(T_2 - T_1)$, and taking, without any real loss of generality, $\omega T_1/b = 2\pi\times$ an integer. This condition (11) is very unlikely to hold in practice because it is the furnace temperature which is controlled and other components, such as the sample pan, will affect the temperature. The second condition follows from the assumption of symmetry about the centre plane $y = 1$. There is also an initial condition given by the periodic solution to (10) - (12) with the final term in (10) set to zero; this applies for any large enough negative τ and comes from having no melting for $T < T_1$.

In [3], two cases and three regimes were found to be significant. The cases were $\lambda \le 1$ and $\lambda > 1$. In the former temperature is always increasing so $\Theta \equiv \theta$ while for the latter $\partial\theta/\partial\tau < 0$ at times and $\Theta > \theta$ for part of each temperature cycle. The two cases were seen to admit slightly different types of behaviour. The three regimes of note were:

Regime 1. Early in the melting process, when there are few, and small, crystals being melted and many remain to take up melt,

$$m(y,\tau,\theta)\frac{\partial\Theta}{\partial\tau} \le f(\theta)\int_\Theta^\infty n^*(\phi)\,\mathrm{d}\phi \qquad \text{and} \qquad \alpha \equiv 0$$

throughout each oscillation.

All melt is recrystallised instantaneously and melting makes no contribution to the heat intake, either for the underlying or the cyclic signal. While this regime applies throughout the sample (the time τ with each point y, $0 < y \le 1$ in Regime 1), the experiment will give no indication of melting, and the sample's temperature remains as the sum of a linear and a periodic function of time.

Regime 2. With a rather higher temperature, so more lamellæ are getting melted,

$$m(y,\tau,\theta)\overline{\frac{\partial\Theta}{\partial\tau}} \equiv m(y,\tau,\theta)\frac{\overline{\partial\theta}}{\partial\tau} < f(\theta)\int_{\Theta}^{\infty} n^*(\phi)\,\mathrm{d}\phi < \max\left\{m(y,\tau,\theta)\frac{\partial\Theta}{\partial\tau}\right\}$$

where the maximum applies over a cycle and $\overline{\ }$ denot= es a time average, also over a cycle, thinking of temperature *etc.* as being approximately periodic over the $\mathrm{O}(1/\Omega)$ time scale of the oscillations. Now net melting does occur, so $\alpha > 0$ for part of each cycle, but the remaining lamellæ are still sufficient to remove all the melt produced during a period so $\alpha = 0$ for part of the time and α remains small.

Regime 3. Later still, with even faster melting – and fewer surviving crystals to remove the amorphous material,

$$f(\theta)\int_{\Theta}^{\infty} n^*(\phi)\,\mathrm{d}\phi \le m(y,\tau,\theta)\overline{\frac{\partial\Theta}{\partial\tau}}\,,$$

and so $\alpha > 0$ throughout each cycle.

If the limiting melt fraction is non-zero, $\alpha^* > 0$, the nature of the regimes is slightly changed, for instance in Regimes 1 & 2, the average melt fraction can change and contribute to the underlying signal.

For the spatially uniform case considered in [3], these three regimes take place successively as time τ goes from 0 (start of melting) to 1 (end of melting). With the temperature varying with position in the current model, melting starts first at $y = 0$ and finally finishes at $y = 1$. In between there can be different zones of $0 < y < 1$ where Regimes 1, 2, 3 apply. The divisions into the two cases, $\lambda \le 1$ or $\lambda > 1$ are also less clear cut when there is spatial dependence. Attenuation of the oscillations away from the surface $y = 0$ means that temperature can sometimes decrease at $y = 0$ but be monotonic increasing in time for values of y close enough to 1.

Much of the analysis of [3] was based on a multiple-scales technique, relying on the high frequency, $\Omega \gg 1$. As well as the dimensionless time τ, which is suitable for looking at the overall behaviour, the fast variable $\sigma = \tau/\Omega$ can be employed in examining changes over the time scale of the oscillations. Temperatures and mass fractions can be sought as functions of both τ and σ, as asymptotic series valid for $\Omega \to \infty$. The leading terms, [3], are seen to be generally independent of σ:

$$\begin{array}{lrcllll}
\text{for } \Omega\to\infty\,, & \theta & \sim & \theta_0(y,\tau) & + & \Omega^{-1}\theta_1(y,\tau,\sigma=) & + \quad \ldots\,,\\
& \Theta & \sim & \Theta_0(y,\tau) & + & \Omega^{-1}\Theta_1(y,\tau,\sigma=) & + \quad \ldots\,,\\
& \alpha & \sim & \alpha_0(y,\tau) & + & \Omega^{-1}\alpha_1(y,\tau,\sigma=) & + \quad \ldots\,,\\
& m & \sim & m_0(y,\tau) & + & \Omega^{-1}m_1(y,\tau,\sigma) & + \quad \ldots\,.
\end{array}$$

These follow from the cyclic term on the boundary, which produces the rapid variation, being $\mathrm{O}(\Omega^{-1})$. The leading underlying terms are simply the leading terms in these expansions. The cyclic behaviour is governed by the $\mathrm{O}(\Omega^{-1})$ terms.

Use of multiple scales

The leading temperature, θ_0, is simply τ on $y = 0$. It follows that θ_0 is monotonic increasing in time so

$$\Theta_0 \equiv \theta_0\,. \tag{13}$$

Generally, the time derivative $\partial/\partial\tau$ is replaced by $\Omega\partial/\partial\sigma + \partial/\partial\tau$. In particular:

$$\text{while } \theta < \Theta\,, \quad \theta_1 < \Theta_1 \text{ and } \frac{\partial\Theta_1}{\partial\sigma} + \frac{\partial\theta_0}{\partial\tau} = 0\,;$$

$$\text{while } \theta = \Theta\,, \quad \theta_1 = \Theta_1 \text{ and } \frac{\partial\Theta_1}{\partial\sigma} + \frac{\partial\Theta_0}{\partial\tau} = \frac{\partial\theta_1}{\partial\sigma} + \frac{\partial\theta_0}{\partial\tau}\,,$$

assuming that the last is positive. Thus

$$\frac{\partial\Theta_1}{\partial\sigma} = \begin{cases} -\dfrac{\partial\theta_0}{\partial\tau} & \text{if } \Theta_1 > \theta_1 \\ \max\left\{-\dfrac{\partial\theta_0}{\partial\tau}, \dfrac{\partial\theta_1}{\partial\sigma}\right\} & \text{if } \Theta_1 = \theta_1 \end{cases}. \tag{14}$$

It should also be noted that $\dfrac{\partial\theta_0}{\partial\tau} = \dfrac{\partial\Theta_0}{\partial\tau} = \overline{\dfrac{\partial\theta_0}{\partial\tau}} = \overline{\dfrac{\partial\Theta_0}{\partial\tau}}$.

The three regimes

In Regime 1, $\alpha_0 \equiv \alpha_1 \equiv 0$ and

$$m_0(y,\tau,\theta_0)\left(\frac{\partial\theta_0}{\partial\tau} + \sup\left\{\frac{\partial\Theta_1}{\partial\sigma}\right\}\right) \leq f(\theta_0)\int_{\theta_0}^{\infty} n^*\,\mathrm{d}\phi\,,$$

(sup, like max above, means the supremum over a period of oscillation).

In Regime 2, $\alpha_0 \equiv 0$,

$$m_0(y,\tau,\theta_0)\frac{\partial\theta_0}{\partial\tau} < f(\theta_0)\int_{\theta_0}^{\infty} n^*\,\mathrm{d}\phi < m_0(y,\tau,\theta_0)\left(\frac{\partial\theta_0}{\partial\tau} + \sup\left\{\frac{\partial\Theta_1}{\partial\sigma}\right\}\right) \tag{15}$$

and α_1 is given by

$$\frac{\partial\alpha_1}{\partial\sigma} = \begin{cases} m_0(y,\tau,\theta_0)\left(\dfrac{\partial\theta_0}{\partial\tau} + \dfrac{\partial\Theta_1}{\partial\sigma}\right) - f(\theta_0)\displaystyle\int_{\theta_0}^{\infty} n^*\,\mathrm{d}\phi & \text{if } \alpha_1 > 0 \\ \max\left\{m_0(y,\tau,\theta_0)\left(\dfrac{\partial\theta_0}{\partial\tau} + \dfrac{\partial\Theta_1}{\partial\sigma}\right) - f(\theta_0)\displaystyle\int_{\theta_0}^{\infty} n^*\,\mathrm{d}\phi\,, 0\right\} & \text{if } \alpha_1 = 0 \end{cases}.$$

In Regime 3, $\alpha_0 > 0$,

$$f(\theta_0)\int_{\theta_0}^{\infty} n^*\,\mathrm{d}\phi \leq m_0(y,\tau,\theta_0)\frac{\partial\theta_0}{\partial\tau} \tag{16}$$

and the melt fraction is given by

$$\frac{\partial\alpha_0}{\partial\sigma} = m_0(y,\tau,\theta_0)\,\frac{\partial\theta_0}{\partial\tau} - f(\theta_0)\int_{\theta_0}^{\infty} n^*\,\mathrm{d}\phi \qquad \text{and} \qquad \frac{\partial\alpha_1}{\partial\sigma} = m_0(y,\tau,\theta_0)\,\frac{\partial\Theta_1}{\partial\sigma}\,. \tag{17}$$

(It is implicit for this categorisation of regimes that (16) holds until melting is, effectively, complete. After such time the material can be regarded as behaving inertly or once again in Regime 1.)

It should be noted that only the leading term of the crystal density, m_0, is important. During Regimes 1 and 2 conservation of mass and the "sharing-out rule" lead to the result

$$m_0(y,\tau,\varphi) = m^*(\varphi) + \frac{\int_0^{\theta_0} m^*(\phi)\,\mathrm{d}\phi}{\int_{\theta_0}^{\infty} n^*(\phi)\,\mathrm{d}\phi} n^*(\varphi) \tag{18}$$

for $\varphi > \theta_0(y,\tau)$, since $\alpha_0 \equiv 0$ during these two regimes; of course $m_0 \equiv 0$ for $\varphi < \theta_0(y,\tau) =$. (The asterisk denotes the initial value for both mass and number densities.)

If the time at which Regime 2 ends and Regime 3 starts is denoted by $\tau = \omega_2(y)$, then in Regime 3 the acquisition of material is given by

$$m_0(y,\tau,\varphi) = m_0(y,\omega_2,\varphi) + n^*(\varphi)\int_{\omega_2}^{\tau} f(\theta(y,\tau'))\,\mathrm{d}\tau'\,. \tag{19}$$

The time ω_2 is fixed by the transition from (15) to (16) while the value $m_0(y,\omega_2,\varphi)$ is determined by (18).

The heat equation

The densities evolve as above while the temperatures θ and Θ are related by (13) and (14) and satisfy

$$\left(\frac{\partial\theta_0}{\partial\tau} + \frac{\partial\theta_1}{\partial\sigma}\right) + \ldots \sim D\frac{\partial^2\theta_0}{\partial y^2} + D\Omega^{-1}\frac{\partial^2\theta_1}{\partial y^2} + \ldots - l\left(\frac{\partial\alpha_0}{\partial\tau} + \frac{\partial\alpha_1}{\partial\sigma}\right) - \ldots \qquad \text{for } 0 < y < 1\,,$$

$$\theta_0 + \Omega^{-1}\theta_1 + \ldots \sim \tau + \lambda\Omega^{-1}\sin\sigma + \ldots \qquad \text{on } y = 0$$

$$\text{and} \qquad \frac{\partial\theta_0}{\partial y} + \Omega^{-1}\frac{\partial\theta_1}{\partial y} + \ldots = 0 \qquad \text{on } y = 1\,.$$

As in the earlier paper, [3], the problem decouples, in the sense that the leading-order problem, *i.e.* that for m_0, α_0, θ_0 and Θ_0, is that for the simpler, "standard" differential scanning calorimetry and can be solved without considering the oscillations.

There are clearly two special cases (or "distinguished limits"):

A. D of order Ω;

B. D of order one.

The latter would give rise to an order-one variation of θ_0 through the sample at any instant of time. This would mean that experimental results for a material with temperature-dependent properties would be difficult to interpret. Moreover, the effect of the rapid oscillations would be confined to a boundary layer of width $\mathrm{O}(\Omega^{-1/2})$ near $y = 0$. There would be a small cyclic signal and relatively high experimental errors.

We therefore first discuss the former case, which is probably the more realistic of the two. For large D, with size Ω, $\theta_0 = \theta_0(\tau)$ and the oscillations are significant throughout the sample: transitions at specific temperatures are more clearly associated with those temperatures while the cyclic signal would be order one, although generally significantly different from the underlying one. (This frequency-dependent effect is seen in practice but can also result from thermal resistances within the calorimeter or pans as well as from the finite thermal conductivity of the sample.)

A. With large D, it can be rescaled, $D = \Omega\mathcal{D}$, and the leading-order temperature satisfies

$$\mathcal{D}\frac{\partial^2\theta_0}{\partial y^2} = 0 \text{ for } 0 < y < 1 \text{ =}, \quad \theta_0 = \tau \text{ on } y = 0\,, \quad \frac{\partial\theta_0}{\partial y} = 0 \text{ on } y = 1\,,$$

$$\text{so } \theta_0 \equiv \tau\,.$$

The first-order correction, θ_1, which should be periodic as a function of the fast time variable σ, is then given by

$$\frac{\partial\theta_1}{\partial\sigma} + 1 = \mathcal{D}\frac{\partial^2\theta_1}{\partial y^2} - l\left(\frac{\partial\alpha_0}{\partial\tau} + \frac{\partial\alpha_1}{\partial\sigma}\right) \text{ for } 0 < y < 1\,,$$

$$\theta_1 = \lambda\sin\sigma \text{ on } y = 0\,, \quad \frac{\partial\theta_1}{\partial y} = 0 \text{ on } y = 1\,.$$

Averaging,

$$\mathcal{D}\frac{\partial^2\overline{\theta}_1}{\partial y^2} = 1 + l\frac{\partial\alpha_0}{\partial\tau} \text{ for } 0 < y < 1\,, \quad \overline{\theta}_1 = 0 \text{ on } y = 0\,, \quad \frac{\partial\overline{\theta}_1}{\partial y} = 0 \text{ on } y = 1 \text{ =}, \tag{20}$$

while the cyclic part of θ_1, $\widetilde{\theta}_1 \equiv \theta_1 - \overline{\theta}_1$, has

$$\frac{\partial\widetilde{\theta}_1}{\partial\sigma} = \mathcal{D}\frac{\partial^2\widetilde{\theta}_1}{\partial y^2} - l\,\frac{\partial\alpha_1}{\partial\sigma} \text{ for } 0 < y < 1\,, \tag{21}$$

$$\widetilde{\theta}_1 = \lambda\sin\sigma \text{ on } y = 0\,, \quad = \frac{\partial\widetilde{\theta}_1}{\partial y} = 0 \text{ on } y = 1\,.$$

Note that because α_0 is independent of σ, $\overline{\alpha}_0 \equiv \alpha_0$, and that α_1 must also be periodic in σ.

The crystalline mass density, given by (18) and (19), simplifies to

$$m_0(y,\tau,\varphi) = m^*(\varphi) + \frac{\int_0^\tau m^*(\phi)\,\mathrm{d}\phi}{\int_\tau^\infty n^*(\phi)\,\mathrm{d}\phi}\,n^*(\varphi) \equiv M_1(\tau,\varphi) \tag{22}$$

in Regimes 1 and 2, and, in Regime 3,

$$m_0(y,\tau,\varphi) = M_1(\omega_2,\varphi) + n^*(\varphi)\int_{\omega_2}^\tau f(\tau')\,\mathrm{d}\tau' \equiv M_3(\tau,\varphi;\omega_2) \quad \text{ for } \tau \geq \omega_2(y)\,. \tag{23}$$

Regime 1 at a point y holds until the time $\tau = \omega_1(y)$ such that

$$M(\tau,\tau)\left(1 + \sup\left\{\frac{\partial\Theta_1}{\partial\sigma}\right\}\right) = f(\tau)\int_\tau^\infty n^*\,\mathrm{d}\phi\,, \tag{24}$$

since now $\theta_0 \equiv \tau$, with θ_1 and Θ_1 given by (14), which here simplifies to

$$\frac{\partial\Theta_1}{\partial\sigma} = \begin{cases} -1 & \text{if } \Theta_1 > \theta_1 \\ \max\left\{-1, \dfrac{\partial\theta_1}{\partial\sigma}\right\} & \text{if } \Theta_1 = \theta_1 \end{cases}. \tag{25}$$

(Note that $\partial\widetilde{\Theta}_1/\partial\sigma \equiv \partial\Theta_1/\partial\sigma$, $\partial\widetilde{\theta}_1/\partial\sigma \equiv \partial\theta_1/\partial\sigma$.)

At the point y, Regime 2 then holds between $\tau = \omega_1(y)$ and $\tau = \omega_2(y) \equiv \tau_3 = \text{const.}$ with

$$f(\tau_3) \int_{\tau_3}^{\infty} n^* \, \mathrm{d}\phi = M_1(\tau_3, \tau_3) \, .$$

Regime 3 applies for $\tau > \tau_3$ (and until the melting has finished).

The zones are sketched in Fig. 2, in which Regimes 1 and 2 are seen to co-exist for $\tau_1 < \tau < \tau_2$, where $\tau_1 = \omega_1(0)$, the time at which the effects of melting are first shown by the cyclic signal, and $\tau_2 = \omega_1(1) < \tau_3$.

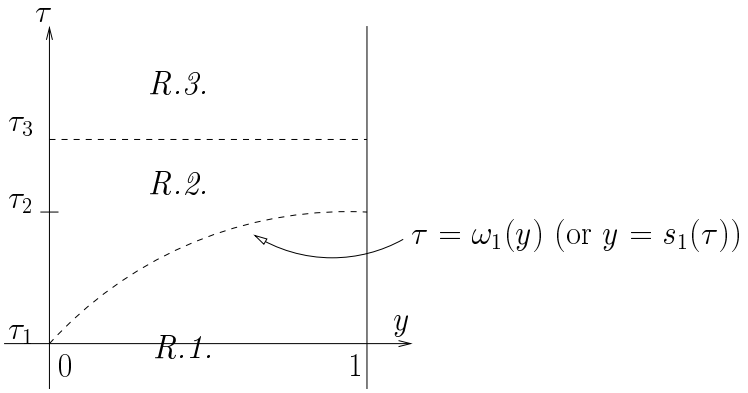

Figure 2: The zones where the three regimes apply for D of order Ω.

The two signals, the measured heat flows into the sample, are finally given by $-D \left. \overline{\dfrac{\partial \theta}{\partial y}} \right|_{y=0} \sim -\mathcal{D} \left. \dfrac{\partial \overline{\theta}_1}{\partial y} \right|_{y=0}$, for the underlying, and, for example, the "amplitude", *e.g.* the square root of the sum of squares of the first Fourier coefficients, of $-D \left. \dfrac{\partial \widetilde{\theta}}{\partial y} \right|_{y=0} \sim -\mathcal{D} \left. \dfrac{\partial \widetilde{\theta}_1}{\partial y} \right|_{y=0=}$, divided by λ, for the cyclic.

B. As D is now order one it is left unscaled. The rapid vari= ation of the cyclic part, with a time scale of $1/\Omega$, is associated with a diffusion length of $1/\Omega^{1/2}$. The oscillations are consequently confined to a boundary layer near $y = 0$ and are negligible for y of order one. In particular, for y not small,

$$\alpha(y, \tau, \sigma) = \alpha(y, \tau) + o(\Omega^{-P}) \quad \text{and} \quad \theta(y, \tau, \sigma) = \Theta(y, \tau, \sigma) = \theta(y, \tau) + o(\Omega^{-P})$$

for $\Omega \gg 1$, with any P. This means that, outside of the boundary layer, Regime 2 fails to exist. Also, in Regime 1,

$$\alpha = 0 \quad \text{and} \quad \frac{\partial \theta}{\partial \tau} = D \frac{\partial^2 \theta}{\partial y^2} \quad \text{with} \quad m(y, \tau, \theta) \frac{\partial \theta}{\partial \tau} < f(\theta) \int_{\theta}^{\infty} n^* \, \mathrm{d}\phi \, , \tag{26}$$

while in Regime 3,

$$\alpha > 0 \, , \quad \frac{\partial \alpha}{\partial \tau} = m(y, \tau, \theta) \frac{\partial \theta}{\partial \tau} - f(\theta) \int_{\theta}^{\infty} n^* \, \mathrm{d}\phi \quad \text{and} \quad \frac{\partial \theta}{\partial \tau} = D \frac{\partial^2 \theta}{\partial y^2} - l \frac{\partial \alpha}{\partial \tau} \, . \tag{27}$$

The change from Regime 1 to Regime 3 at a point y happens at $\tau = \omega_3(y)$ determined by

$$m(y, \tau, \theta) \frac{\partial \theta}{\partial \tau} = f(\theta) \int_{\theta}^{\infty} n^* \, \mathrm{d}\phi \, .$$

With the negligible effect of the oscillations outside the boundary layer, the required boundary conditions are, to leading order,

$$\theta = \tau \ \text{ on } \ y = 0 \quad \text{and} \quad \frac{\partial \theta}{\partial y} = 0 \ \text{ on } \ y = 1 \, . \tag{28}$$

Note that while all the sample lies in Regime 1,

$$\theta \sim \tau - \frac{2y - y^2}{2D} \tag{29}$$

and Regime 3 first starts at $y = 0$ near the time $\tau = \tau_2 = \omega_3(0)$ given by

$$m(0, \tau, \tau) = f(\tau) \int_{\tau}^{\infty} n^* \, \mathrm{d}\phi \, ,$$

see Fig. 3.

Regimes 1 and 3 could be combined by writing

$$\frac{\partial\alpha}{\partial\tau} = \max\left\{ m(y,\tau,\theta)\frac{\partial\theta}{\partial\tau} - f(\theta)\int_\theta^\infty n^*\,\mathrm{d}\phi\,, 0\right\}\,, \quad \frac{\partial\theta}{\partial\tau} = D\frac{\partial^2\theta}{\partial y^2} - l\frac{\partial\alpha}{\partial\tau}\,; \tag{30}$$

m is still given by (18) and (19), but with ω_2 replaced by ω_3, and θ_0 by θ, in the two r= egimes.

In the boundary layer, $y = \Omega^{-1/2}z$ and $\theta \sim \tau - \Omega^{-1/2}A(\tau)z + \Omega^{-1}\theta_1 + \ldots$. The second term in the expansion of θ is required to ensure matching with the outer solution (26) or (27). The problem for the leading-order oscillatory term is here

$$\frac{\partial\widetilde{\theta}_1}{\partial\sigma} = D\frac{\partial^2\widetilde{\theta}_1}{\partial z^2} - l\frac{\partial\alpha_1}{\partial\sigma}$$

with

$$\alpha_1 \equiv 0 \quad \text{in Regime 1 and}$$

$$\frac{\partial\alpha_1}{\partial\sigma} = \begin{cases} M_1(\tau,\tau)\left(1+\dfrac{\partial\widetilde{\Theta}_1}{\partial\sigma}\right) - f(\tau)\displaystyle\int_\tau^\infty n^*\,\mathrm{d}\phi & \text{for } \alpha_1 > 0 \\ \\ \max\left\{ M_1(\tau,\tau)\left(1+\dfrac{\partial\widetilde{\Theta}_1}{\partial\sigma}\right) - f(\tau)\displaystyle\int_\tau^\infty n^*\,\mathrm{d}\phi\,, 0\right\} & \text{for } \alpha_1 = 0 \end{cases} \quad \text{in Regime 2.}$$

In Regime 3

$$\frac{\partial\widetilde{\theta}_1}{\partial\sigma} = D\frac{\partial^2\widetilde{\theta}_1}{\partial z^2} - lM_3(\tau,\tau;\tau_2)\,\frac{\partial\widetilde{\Theta}_1}{\partial\sigma}\,, \tag{31}$$

since $\theta_0 = \Theta_0 = \tau$ in this boundary layer. The relation (25) again holds.

Regime 1 applies up to the time $\tau = \omega_1(z)$ at which

$$M_1(\tau,\tau)\left(1+\sup\left\{\frac{\partial\widetilde{\Theta}_1}{\partial\sigma}\right\}\right) = f(\tau)\int_\tau^\infty n^*\,\mathrm{d}\phi\,,$$

Regime 2 holds for $\omega_1(z) < \tau < \tau_2 = \omega_3(0)$, and Regime 3 for $\tau > \tau_2$, see Fig. 3. ($\omega_1 \to \tau_2$ as $z \to \infty$.) Note that the whole boundary layer, and therefore the whole sample, is in Regime 1 up to the time $\tau = \tau_1 = \omega_1(0)$,

$$M_1(\tau_1,\tau_1)\,(1+\lambda^*) = f(\tau_1)\int_{\tau_1}^\infty n^*\,\mathrm{d}\phi\,,$$

since the oscillations will be largest on the boundary, $z = y = 0$. Here $\lambda^* = \sup\left\{\dfrac{\partial\Theta_1^*}{\partial\sigma}\right\}$, where Θ_1^* is given by

$$\frac{\partial\Theta_1^*}{\partial\sigma} = \begin{cases} -1 & \text{if } \Theta_1 > \lambda\sin\sigma \\ \\ \max\{-1, \lambda\sin\sigma\} & \text{if } \Theta_1 = \lambda\sin\sigma \end{cases}\,.$$

For sufficiently small λ, certainly $\lambda \le 1$, $\lambda^* = \lambda$.

In case **B** the underlying signal is

$$-D\left.\overline{\frac{\partial\theta}{\partial y}}\right|_{y=0} \sim DA(\tau) = -\left.D\frac{\partial\overline{\theta}_0}{\partial y}\right|_{y=0}\,,$$

where this θ_0 is the solution of the outer problem, say (30) and (28), and the cyclic signal is given in terms of

$$-\left.D\frac{\partial\widetilde{\theta}}{\partial y}\right|_{y=0} \sim -D\Omega^{-1/2}\left.\frac{\partial\widetilde{\theta}_1}{\partial z}\right|_{z=0}\,,$$

where $\widetilde{\theta}_1$ solves the boundary-layer problem.

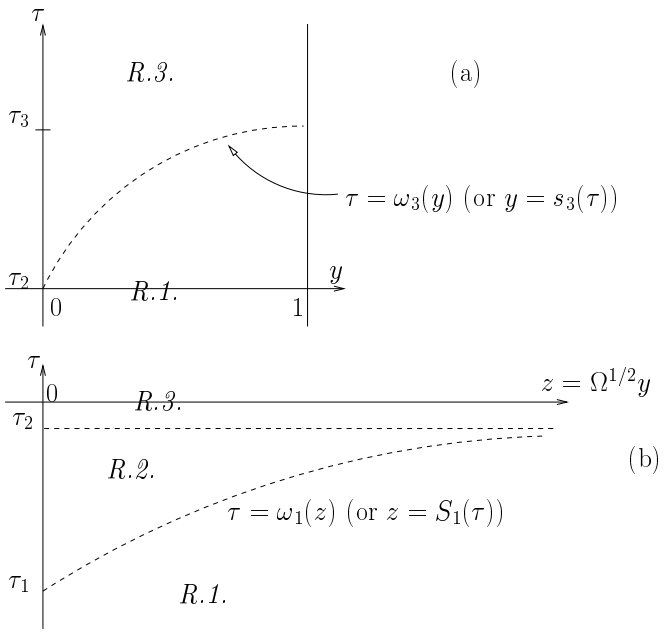

Figure 3: The two surviving regimes in the outer region, (a), and all three in the boundary layer, (b), for D of order one.=

4 Analysis and Implications of the Model

This section is devoted to the consequences of the models derived, and partially analysed, in the previous two. The discussion here is qualitative, in contrast with the numerical results presented in the following section, and treats the large-diffusivity case, **A**, and the order-one-diffusivity case, **B**, separately. The distinction between smaller ($\lambda \leq 1$) and larger ($\lambda > 1$) amplitude is not so significant here as it was in [3] because in Regime 2 the manner of oscillation of the melt fraction α (in part of each cycle it is identically zero) prevents θ and Θ from varying sinusoidally. Also, on account of the attenuation of oscillations going into the sample, it is possible, even if $\lambda > 1$, to have θ always increasing in time, deeper within the sample. When Regime 3 is present and 2 is absent, having $\lambda \leq 1$ does, however, make it easier to obtain analytical solutions as in this case θ and Θ do behave sinusoidally.

Little can be obtained analytically when part of the sample is in Regime 2, or part lying in Regime 3 experiences sometimes decreasing temperature, because of the non-sinusoidal variation.

A. Towards the start, $\tau < \tau_1$, the whole sample lies in Regime 1 so $\alpha_0 \equiv 0$, $\alpha_1 \equiv 0$, $\overline{\theta}_1 = -(2y - y^2)/2\mathcal{D}$ (from (20), *c.f.* (29)) and

$$\frac{\partial \widetilde{\theta}_1}{\partial \sigma} = D \frac{\partial^2 \widetilde{\theta}_1}{\partial y^2} \qquad \text{in } 0 < y < 1 \tag{32}$$

with

$$\widetilde{\theta}_1 = \lambda \sin \sigma \qquad \text{on } y = 0 \qquad \text{and} \qquad \frac{\partial \widetilde{\theta}_1}{\partial y} = 0 \qquad \text{on } y = 1\,. \tag{33}$$

This cyclic part can be written as $\widetilde{\theta}_1 = \mathrm{Re}\{\widehat{\theta}_1(y) e^{\mathrm{i}\sigma}\}$ with the complex amplitude satisfying $\mathcal{D}\mathrm{d}^2\widehat{\theta}_1/\mathrm{d}y^2 = \mathrm{i}\widehat{\theta}_1$ along with, from (33), $\widehat{\theta}_1(0) = -\mathrm{i}\lambda$ and $\dfrac{\mathrm{d}\widehat{\theta}_1}{\mathrm{d}y}(1) = 0$ so

$$\widehat{\theta}_1 = \frac{-\mathrm{i}\lambda \cosh((1+\mathrm{i})(1-y)/\sqrt{2\mathcal{D}})}{\cosh((1+\mathrm{i})/\sqrt{2\mathcal{D}})}\,.$$

The dimensionless measurements are then 1 for the underlying signal and $\dfrac{\mathcal{D}}{\lambda}\left|\dfrac{\mathrm{d}\widetilde{\theta}_1}{\mathrm{d}y}(0)\right| = \sqrt{\mathcal{D}}\left|\tanh\left(\dfrac{1+\mathrm{i}}{\sqrt{2\mathcal{D}}}\right)\right|$ for the cyclic signal. Multiplying by the appropriate scaling factor to recover the dimensional value, simply the true specific heat c, the underlying signal is

$$\mathcal{U} = c$$

and the cylic signal is

$$\mathcal{C} = c\sqrt{\mathcal{D}}\left|\tanh\left(\frac{1+\mathrm{i}}{\sqrt{2\mathcal{D}}}\right)\right| . \tag{34}$$

Note that for large $\mathcal{D}$ ("lowish" frequencies) the cyclic signal reduces to the correct value, c, but for small $\mathcal{D}$ ("highish" frequencies) it is an underestimate, $\sqrt{\mathcal{D}}\,c$.

For $\tau_1 < \tau < \tau_3$, so that some or all of the sample is in Regime 2, the cyclic signal is again given by the first Fourier coefficients of $\left.\dfrac{\partial\widetilde{\theta}_1}{\partial y}\right|_{y=0}$ but this oscillatory part of the temperature cannot now be found explicitly. In $\tau_2 < \tau < \tau_3$, $\widetilde{\theta}_1$ satisfies (21) with (33). For $\tau_1 < \tau < \tau_2$, (21) only applies in $0 < y < s_1(\tau) = \omega_1^{-1}(\tau)$ with (32) holding in $s_1(\tau) < y < 1$; $\widetilde{\theta}_1$ and $\partial\widetilde{\theta}_1/\partial y$ are continuous at $y = s_1$. The effect of the varying α_1 term in (21) will increase the cyclic signal. Throughout $\tau_1 < \tau < \tau_3$, with none of the sample in Regime 3, the underlying signal maintains the correct value c.

For $\tau > \tau_3$, the whole sample is in Regime 3 and the melt fraction $\alpha_0 = \alpha_0(\tau) > 0$ is found from

$$\frac{\mathrm{d}\alpha_0}{\mathrm{d}\tau} = M_3(\tau,\tau;\tau_3) - f(\tau)\int_\tau^\infty n^*\,\mathrm{d}\phi\,.$$

The dimensionless underlying temperature, from (20), is now

$$\overline{\theta} \sim \tau - \left(\frac{2y-y^2}{2\Omega^{1/2}\mathcal{D}}\right)\left(1 + l\frac{\mathrm{d}\alpha_0}{\mathrm{d}\tau}\right)\ldots$$

so the underlying signal is, approximately,

$$\mathcal{U} \sim c + cl\frac{\mathrm{d}\alpha_0}{\mathrm{d}\tau} = c + \frac{L}{T_2-T_1}\frac{\mathrm{d}\alpha_0}{\mathrm{d}\tau} = c + \frac{L}{b}\frac{\mathrm{d}\alpha_0}{\mathrm{d}t}\,.$$

Meanwhile the oscillatory temperature is, in principle at least, found from (21), (17) and (23):

$$\frac{\partial\widetilde{\theta}_1}{\partial\sigma} = \mathcal{D}\frac{\partial^2\widetilde{\theta}_1}{\partial y^2} - lM_3(\tau,\tau;\tau_3)\frac{\partial\widetilde{\Theta}_1}{\partial\sigma}\,.$$

For small amplitudes, $\lambda \leq 1$ so that the temperature is increasing in time throughout, $\widetilde{\Theta}_1 \equiv \widetilde{\theta}_1$ and, following the results for $\tau < \tau_1$,

$$\widehat{\theta}_1 = \frac{-\mathrm{i}\lambda\cosh((1+\mathrm{i})\sqrt{1+lM_3}\,(1-y)/\sqrt{2\mathcal{D}})}{\cosh((1+\mathrm{i})\sqrt{1+lM_3}\,/\sqrt{2\mathcal{D}})}\,,$$

giving a cyclic signal

$$\mathcal{C} \sim c\sqrt{\mathcal{D}(1+lM_3(\tau,\tau;\tau_3))}\left|\tanh\left((1+\mathrm{i})\sqrt{\frac{1+lM_3(\tau,\tau;\tau_3)}{2\mathcal{D}}}\right)\right| .$$

To obtain a more explicit result, it is necessary to have specific, and ideally simple, functions appearing in the model. We here suppose for this case **A** with $\lambda \leq 1$, that

$$f(\theta) = a = \text{const.} > 1 \qquad \text{and} \qquad n^*(\varphi) = m^*(\varphi) = \begin{cases} 0 & \text{for } \varphi < 0 \\ 1 & \text{for } 0 < \varphi < 1 \\ 0 & \text{for } \varphi > 1 \end{cases} .$$

Further assumptions will be made shortly.

Then, in Regimes 1 and 2 ($\tau < \tau_3$),

$$m_0(y,\tau,\varphi) = M_1(\tau,\varphi) = 1 + \frac{\int_0^\tau \mathrm{d}\phi}{\int_\tau^1 \mathrm{d}\phi} = \frac{1}{1-\tau} \quad \text{for } \tau < \varphi < 1$$

and 0 otherwise. At $\tau = \tau_3$,

$$M_1(\tau_3,\tau_3) = \frac{1}{1-\tau_3} = a\int_{\tau_3}^1 \mathrm{d}\phi = a(1-\tau_3) \quad \text{so } \tau_3 = 1 - 1/\sqrt{a}\,.$$

In Regime 3 ($1 - 1/\sqrt{a} < \tau < 1$),

$$m_0(y,\tau,\varphi) = M_3(\tau,\varphi;\tau_3) = \sqrt{a} + a\int_{1-1/\sqrt{a}}^\tau \mathrm{d}\tau_1 = a\tau - a + 2\sqrt{a}$$

for $\tau < \varphi < 1$, and 0 otherwise. Then, for $1 - 1/\sqrt{a} < \tau < 1$, the dimensionless underlying signal is

$$\mathcal{U}' = 1 + l((a\tau - a + 2\sqrt{a}) - a(1-\tau)) = 1 + 2l(a\tau - a + \sqrt{a})$$

which increases linearly from 1, its value in Regimes 1 and 2, to $1+2l\sqrt{a}$. Over the same time, the corresponding cyclic signal is

$$\mathcal{C}' = \sqrt{\mathcal{D}(1 + l(a\tau - a + 2\sqrt{a}))}\left|\tanh\left((1+\mathrm{i})\sqrt{\frac{1 + l(a\tau - a + 2\sqrt{a})}{2\mathcal{D}}}\right)\right| .$$

The qualitative behaviour is not immediately clear, for general a, l and $\mathcal{D}$. A limiting version of this prototype model can be considered, taking $\mathcal{D}$ and l large, with $\mathcal{D} = \beta^2 l$ for some fixed β. Now

$$\mathcal{U}' \sim 2l(a\tau - a + \sqrt{a})$$

increases from nearly 0 (compared with l) to $2l\sqrt{a}$. Also

$$\mathcal{C}' \sim \beta l\sqrt{a\tau - a + 2\sqrt{a}}\left|\tanh\left(\frac{(1+\mathrm{i})}{\beta}\sqrt{\frac{a\tau - a + 2\sqrt{a}}{2}}\right)\right| .$$

At the start of Regime 3 this is $\beta l a^{1/4}\left|\tanh\left(\dfrac{(1+\mathrm{i})a^{1/4}}{\sqrt{2}\beta}\right)\right|$, which is of order l. At the finish, $\tau = 1$,

$$\mathcal{C}' \sim \sqrt{2}\beta l a^{1/4}\left|\tanh\left(\frac{(1+\mathrm{i})a^{1/4}}{\beta}\right)\right|$$

and then

$$\left(\frac{\mathcal{C}}{\mathcal{U}}\right)^2 = \left(\frac{\mathcal{C}'}{\mathcal{U}'}\right)^2 \sim \frac{\beta^2}{2\sqrt{a}}\left|\tanh\left(\frac{(1+\mathrm{i})a^{1/4}}{\beta}\right)\right|^2 = G(X) \equiv \frac{2}{X^2}\left(\frac{\cosh X - \cos X}{\cosh X + \cos X}\right)$$

where $X = 2a^{1/4}/\beta$. Since $G(X) < 1$ for $X > 0$, $\mathcal{C} < \mathcal{U}$ at $\tau = 1$ and it follows that, in this very specialised and probably rather unrealistic case, the two signals cross, something like the sketch in Fig. 4. (Note that $G(X) < 1$ is physically intuitive as it gives the square of the ratios of the two signals for an inert material, with constant specific heat, and with a finite thermal diffusivity.) Fig. 4 is, very roughly, in agreement with the forms found in real experiments except that the approximately triangular shapes seen here are artifacts of the uniform initial densities n^* and m^*.

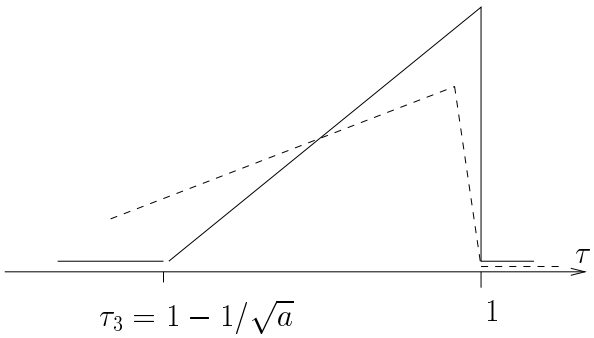

Figure 4: Sketch of the underlying (solid line) and cyclic (broken line) signals during Regime 3 for the model problem.

More realistic profiles might be given by taking $f(\theta) \equiv a > 0$, as before, but now $m^*(\varphi) = Mh(\varphi)$, $n^*(\varphi) = Nh(\varphi)$, for some positive constants M and N, with a distribution function $h \equiv 0$ for $\varphi \le 0$ and for $\varphi \ge 1$ but $h > 0$ for $0 \le \varphi \le 1$ (see Fig. 5); h can be normalised so that $\int h(\phi)\,\mathrm{d}\phi = 1$. Proceeding much as just above, for $0 < \tau < \varphi < 1$,

$$m = M_1(\tau, \varphi) = M\left(1 + \frac{\int_0^\tau h\,\mathrm{d}\phi}{\int_\tau^1 h\,\mathrm{d}\phi}\right)h(\varphi)$$

when $\tau \le \tau_3$, which is given by

$$M\left(1 + \frac{\int_0^{\tau_3} h\,\mathrm{d}\phi}{\int_{\tau_3}^1 h\,\mathrm{d}\phi}\right)h(\tau_3) = aN\int_{\tau_3}^1 h\,\mathrm{d}\phi\,, \quad \textit{i.e.}\ \frac{Mh(\tau_3)}{aN} = \left(\int_{\tau_3}^1 h\,\mathrm{d}\phi\right)^2 ,$$

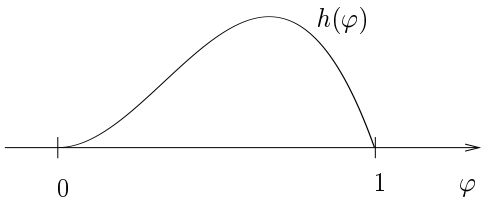

Figure 5: A scaled density function for a model problem.

and then

$$m = M_3(\tau,\varphi) = \left(\frac{M}{\int_{\tau_3}^1 h \,\mathrm{d}\phi} + Na(\tau-\tau_3) \right) h(\varphi) = aN \left(\frac{\int_{\tau_3}^1 h \,\mathrm{d}\phi}{h(\tau_3)} + \tau - \tau_3 \right) h(\varphi)$$

when $\tau \geq \tau_3$.

Again taking $\mathcal{D} \gg 1$, $l \gg 1$ with $\mathcal{D} = \beta^2 l$,

$$\mathcal{U}' \sim l \left(M_3(\tau,\tau) - aN \int_\tau^1 h \,\mathrm{d}\phi \right)$$

$$\text{and} \qquad \mathcal{C}' \sim \beta l \sqrt{M_3(\tau,\tau)} \left| \tanh\left(\left(\frac{1+\mathrm{i}}{\beta} \right) \sqrt{\frac{M_3(\tau,\tau)}{2}} \right) \right| .$$

Typical forms of $M_3(\tau,\tau)$, $\mathcal{U}'$ and $\mathcal{C}'$ are as sketched in Fig. 6. Note that $\mathcal{C}' \sim l M_3(\tau,\tau) \to 0$ for $\tau \to 1-$. The

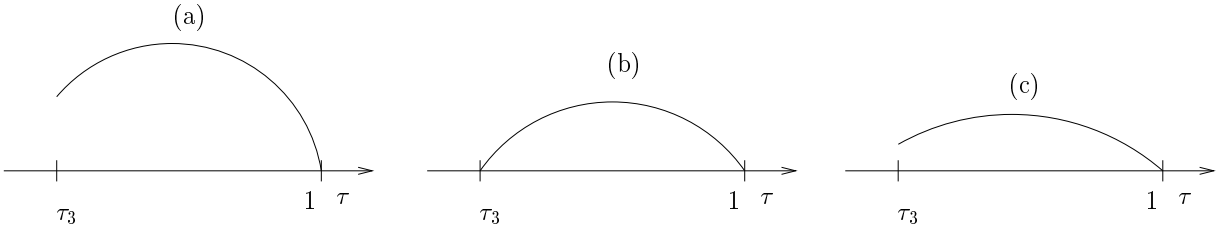

Figure 6: Sketches of profiles of (a) $M_3(\tau,\tau)$, (b) the underlying signal $\mathcal{U}'$ and (c) the cyclic signal $\mathcal{C}'$.

limiting case of $\beta \to \infty$ gives $\mathcal{C}' = l M_3(\tau,\tau) > \mathcal{U}'$, as in [3]. However, for finite β, $\mathcal{C}' < l M_3(\tau,\tau)$. (Indeed, taking $\beta \to 0$, $\mathcal{C}' \sim \beta l \sqrt{M_3(\tau,\tau)}$.) It is apparent that for some finite (order one) β, so that $\mathcal{D}$ is large enough compared to l, the signals $\mathcal{U}$ and $\mathcal{C}$ will cross at some time τ between τ_3 and 1.

B. For $\tau < \tau_2$, so only Regimes 1 and 2 apply, the outer solution has $\theta_0 = 1 - (2y - y^2)/2D$ so the dimensional underlying signal is approximately

$$\mathcal{U} \sim cD \left. \frac{\partial \theta_0}{\partial y} \right|_{y=0} = c \,.$$

For $\tau < \tau_1$, so that the whole sample is in Regime 1, the perturbation to the temperature in the boundary layer satisfies $\widetilde{\theta}_1 = \mathrm{Re}\{\widehat{\theta}_1(z) e^{\mathrm{i}\sigma}\}$ with

$$\frac{\mathrm{d}^2 \widehat{\theta}_1}{\mathrm{d}z^2} = D \widehat{\theta}_1 \quad \text{for } z > 0 \,, \quad \widehat{\theta}_1 = -\mathrm{i}\lambda \quad \text{on } z = 0 \,, \quad \widetilde{\theta}_1 \to 0 \text{ as } z \to \infty \,.$$

It follows that $\widehat{\theta}_1 = -\mathrm{i}\lambda e^{-(1+\mathrm{i})z/\sqrt{2D}}$ and the cyclic signal is, to leading order,

$$\frac{cD\Omega^{-1/2}}{\lambda} \left| \frac{\partial \widehat{\theta}_1}{\partial z} \right| = c\sqrt{\frac{D}{\Omega}} = \frac{1}{\ell} \sqrt{\frac{kc}{\rho\omega}} \,,$$

which is, of course, a gross underestimate. For $\tau_1 < \tau < \tau_2$, part of the boundary layer is in Regime 2 and it is not possible to solve the problem for $\widetilde{\theta}_1$ exactly. It is clear, however, that the cyclic signal will still have the $\Omega^{-1/2}$ frequency dependence but will be boosted through the effect of the (non-dimensional) latent heat, l.

In the time interval $\tau_2 < \tau < \tau_3$, θ_0 is given by (18), (19) (with ω_3 in place of ω_2), (30) and (28). The effect of the latent heat, through the last term in (30), enlarges the underlying signal. Now the cylic perturbation satisfies (31) in the boundary layer. For $\lambda > 1$, $\widetilde{\Theta}_1 \neq \widetilde{\theta}_1$ for z too small, so again the problem cannot be solved

analytically but it is clear that the cyclic signal is $\mathrm{O}(\Omega^{-1/2})$ and increases with l. For $\lambda \leq 1$, $\widetilde{\Theta}_1 = \widetilde{\theta}_1$ for all z and $\widetilde{\theta}_1 = \mathrm{Re}\left\{-\mathrm{i}\lambda \exp\left[-(1+\mathrm{i})z\sqrt{(1+lM_3)/2D}\right]\right\}$. It follows that the cyclic measurement is now

$$\left(\frac{cD}{\lambda\Omega^{1/2}}\right)\left(\lambda\sqrt{\frac{1+lM_3}{D}}\right) = c\sqrt{\frac{D(1+lM_3)}{\Omega}} = \frac{1}{\ell}\sqrt{\frac{kc}{\rho\omega}\left(1+\frac{L}{c(T_2-T_1)}M_3\right)} \quad ,$$

where M_3, given by (23), is determined by the crystalisation rate F, the densities $\mathcal{N}$ and $\mathcal{M}$, and the experiment-dependent scaling constants such as the ramp b.

5 Numerical Solution

We solve the system of equations (8), (9), (10), modelling polymer crystal density, mass fraction and temperature, using a simple finite difference scheme. For convenience, we rewrite the equations, introducing two indicator variables p and q with $p = 0$ where $\alpha = 0$, $p = 1$ where $\alpha > 0$, $q = 0$ where $\Theta > \theta$, $q = 1$ where $\Theta = \theta$:

$$\frac{\partial m}{\partial \tau}(y,\tau) = pf(\theta)n^*(\varphi) + (1-p)\frac{m(y,\tau,\theta)n^*(\varphi)}{\int_\Theta^\infty n^*\,\mathrm{d}\phi}\frac{\partial \Theta}{\partial \tau}\,, \tag{35}$$

with $m(y,\tau_0,\varphi) = m^*(\varphi)$,

$$\frac{\partial \alpha}{\partial \tau}(y,\tau) = pm(y,\tau,\theta)\frac{\partial \Theta}{\partial \tau} - pf(\theta)\int_\Theta^\infty n^*\,\mathrm{d}\phi, \tag{36}$$

with $\alpha(y,\tau_0) = 0$, and

$$\frac{\partial \theta}{\partial \tau} = D\frac{\partial^2 \theta}{\partial y^2} - l\frac{\partial \alpha}{\partial \tau}\,, \tag{37}$$

with $\theta(0,\tau) = \tau + (\lambda/\Omega)\sin\Omega\tau$ on $y = 0$, $\partial\theta/\partial y = 0$ on $y = 1$, and

$$\theta(y,\tau_0) = \tau_0 - \left(\frac{2y-y^2}{2D}\right) - \lambda\mathrm{Re}\left\{\frac{\mathrm{i}\cosh(\sqrt{\Omega/2D}\,(1+\mathrm{i})(1-y))}{\cosh(\sqrt{\Omega/2D}\,(1+\mathrm{i}))}\,e^{\mathrm{i}\Omega\tau_0}\right\} \quad \text{at } \tau = \tau_0\,.$$

Here τ_0 is chosen so that $\theta \leq 0$ (melting has yet to start) for $\tau \leq \tau_0$, *e.g.* $\tau_0 = -\lambda$.

We apply a discretization in the space interval $[0,1]$ so that the jth point in our discretization is $y_j = j\,\delta y$, for δy the length of a space grid, and also in the range of temperature where the simulation is required, *i.e.* in $[0,1]$, so that $\varphi_k = k\,\delta\varphi$.

Combining equations (36) and (37) we can compute the evolution of m, α and θ in time for $0 < y < 1$, using the following finite difference approximations. First, for temperature $\theta_j^i = \theta(j\,\delta y, i\,\delta\tau)$,

$$\theta_j^{i+1} = \theta_j^i + \frac{\delta\tau}{(q_j^i\,p_j^i\,l\,m_j'^i + 1)}\left[\frac{D}{(\delta y)^2}(\theta_{j+1}^i - 2\theta_j^i + \theta_{j-1}^i) + lp_j^i\,f(\theta_j^i)\,I_j^i\right] \tag{38}$$

where $I_j^i = \int_{\Theta_i^j}^\infty n^*(\phi)\,\mathrm{d}\phi$, $m_j^{i,k} = m(j\,\delta y, i\,\delta\tau, \varphi_k)$, $m_j'^i = m(j\,\delta y, i\,\delta\tau, \theta_j^i)$ and $\delta\tau$ the time step. The values of m' are got from those of m by interpolation. The integral I_j^i can be evaluated by Simpson's rule. Note that $\Theta_j^i = \max\{\theta_j^s, 0 < s < i,\, s \in \mathbb{N}\}$ and that we have used the relation $(\Theta_j^{i+1} - \Theta_j^i)/\delta\tau = q_j^i(\theta_j^{i+1} - \theta_j^i)/\delta\tau$ where $q_j^i = 0$ for $\Theta_j^i > \theta_j^i$ and $q_j^i = 1$ for $\Theta_j^i \leq \theta_j^i$. In addition $p_j^i = 1$ for $\alpha_j^i > 0$ and $p_j^i = 0$ for $\alpha_j^i = 0$. Next, the crystal density is approximated using

$$m_j^{i+1,k} = m_j^{i,k} + \left(\delta\tau\,p_j^i f(\theta_j^i)n^k + (1-p_j^i)\frac{m_j'^{i,k}\,n^k}{I_j^i}q_j^i(\theta_j^{i+1} - \theta_j^i)\right). \tag{39}$$

Here $n^k = n^*(\varphi_k)$. Finally, the melt fraction is got from

$$\alpha_j^{i+1} = \alpha_j^i + p_j^i\,q_j^i\,m_j'^i(\theta_j^{i+1} - \theta_j^i) - \delta\tau\,p_j^i\,I_j^i\,. \tag{40}$$

Three sets of results are shown here. All are done for $f \equiv 1$, $\Omega = 300$ and $l = 0.1$. The dimensionless frequency, Ω, used is somewhat on the high side, a value of 100 might be more realistic, [3], but the larger figure was employed here to be able to see the different regimes more clearly. The dimensionless density functions $n^*(\varphi)$ and $m^*(\varphi)$ were both assumed to be normal: $n^* = m^* = \dfrac{1}{\sqrt{2\pi}\,\sigma}\exp\left(-\dfrac{(\varphi-\mu)^2}{2\sigma^2}\right)$, with $\sigma = 0.15$ and

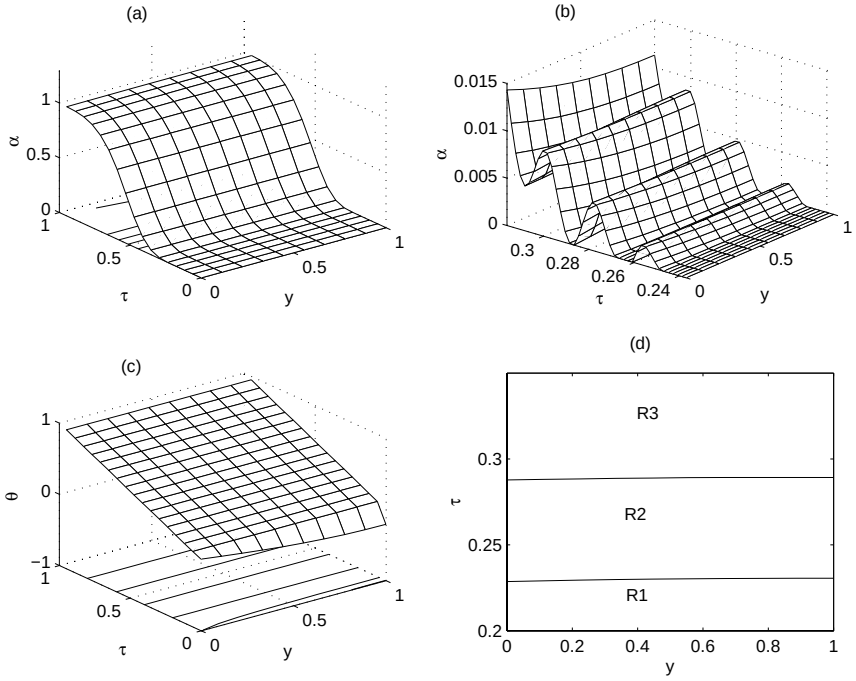

Figure 7: Simulations of the melt fraction α, (a) and (b), dimensionless temperature θ, (c), and the three regimes for $D = 300$ and $\lambda = 0.9$.

$\mu = 0.5$. The numbers and mass of lamellæ with dimensionless melting temperature outside $0 < \varphi < 1$ are then negligible.

The first set of results are for D of order Ω with $\lambda < 1$. The results, for a space step $\delta y = 0.05$ and time step $\delta t = 10^{-6}$, for melt fraction, (a), with a blow-up of Regime 2, (b), temperature, (c), and the location of the three regimes, (d), are shown in Fig. 7 while Fig. 8 shows the simulations of the dimensionless signals (measured values of specific heat). Note that the (underlying) temperature and melt fraction are nearly independent of position y and that the two signals cross as required.

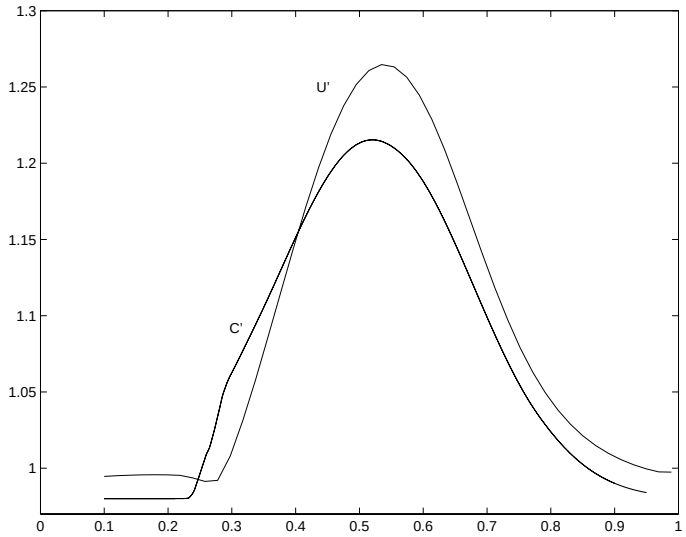

Figure 8: Simulations of the dimensionless underlying, $\mathcal{U}'$, and cyclic, $\mathcal{C}'$, signals for $D = 300$ and $\lambda = 0.9$.

Corresponding results for $\lambda > 1$ are given in Figs. 9 and 10. They are seen to be qualitatively the same as those for the smaller value of λ. The space step was again 0.05 and time step was again 10^{-6}.

The final simulations are for D of order one and $\lambda < 1$ and are shown in Figs. 11 and 12. It is now seen that the underlying melt fraction and temperature vary significantly with position. It can also be observed that the oscillatory behaviour, Fig. 11 (b), and Regime 2, Fig. 11 (d), are confined to a boundary layer near $y = 0$. The

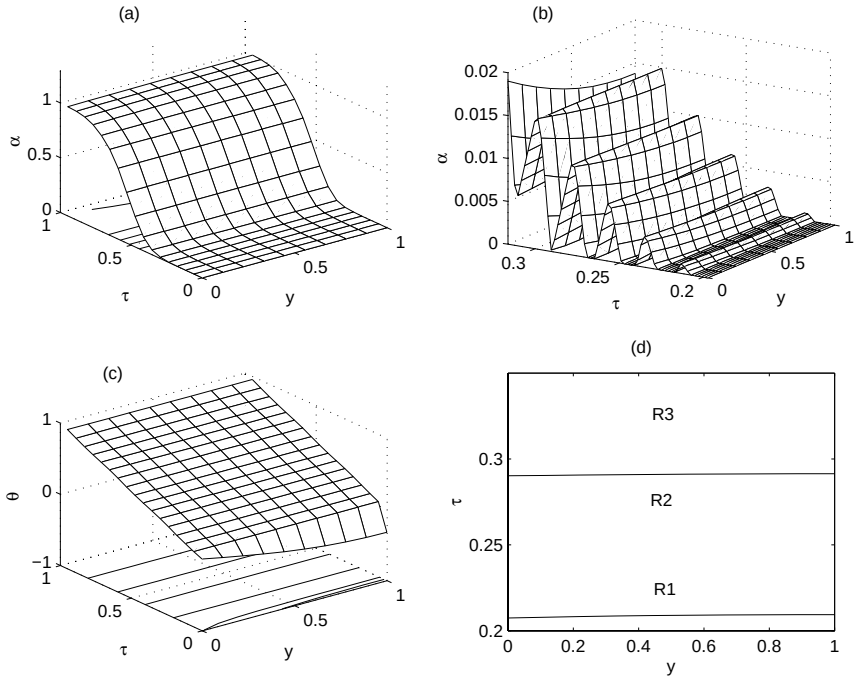

Figure 9: Simulations of the melt fraction α, (a) and (b), dimensionless temperature θ, (c), and the three regimes for $D = 1$ and $\lambda = 2$.

cyclic signal, Fig. 12, is very much smaller than the true value of specific heat. Here the space step was 0.04 and time step was 1.536×10^{-4}.

Computions were also carried out for D of order one and $\lambda > 1$ but they are not shown here because the results were very similar to Figs. 11 and 12.

6 Discussion

The melting of a polymer has been modelled, as a one-dimensional slab, by considering it as consisting of lamellæ, with a range of different melting points. The lamellæ melt the instant their melting point is exceeded while those with higher melting temperatures gradually grow by taking up available melt. We have assumed that the process occurs fast enough for nucleation to be neglected. The model was analysed by using multiple scales. The reduced model can be used to study the three key regimes: 1, where the melt fraction remains identically zero; 2, where it is negligible as far as the overall, or underlying, behaviour is concerned but small variations are important for cyclic measurements; and 3, where the melt increases significantly and its rate of change affects both underlying and cyclic signals. This gives an understanding of the dynamics of the process and relates, both qualitatively and quantitatively, distributions and rates to signals. The problem was solved numerically by using a forward finite difference scheme and the results were in agreement with our asymptotic analysis. Finally, the MTDSC signal was also simulated and it was seen that for a sample with large diffusion, comparable with the large size of frequency, the underlying and cyclic measurements of heat capacity had the same qualitative behaviour as in real experiments.

It was assumed throughout that the forms of the rate function *etc.* were such that the sample would go from Regime 1 to 2 and then to 3, but not *vice versa*.

References

[1] K. J. Jones, I. Kinshott, M. Reading, A. A. Lacey, C. Nikolopoulos, and H. M. Pollock, *The origin and interpretation of the signals of MTDSC*, Thermochemica Acta, 304/305 (1997), pp. 187–199.

[2] A. A. Lacey, C. Nikolopoulos, and M. Reading, *A mathematical model for modulated differential scanning calorimetry*, J. Therm. Anal., 50 (1997), pp. 279–333.

[3] A. A. Lacey, and C. Nikolopoulos, *A model for polymer melting during modulated differential scanning calorimetry*, IMA Journal of Appl. Math. 66 (2001), pp. 449–476.

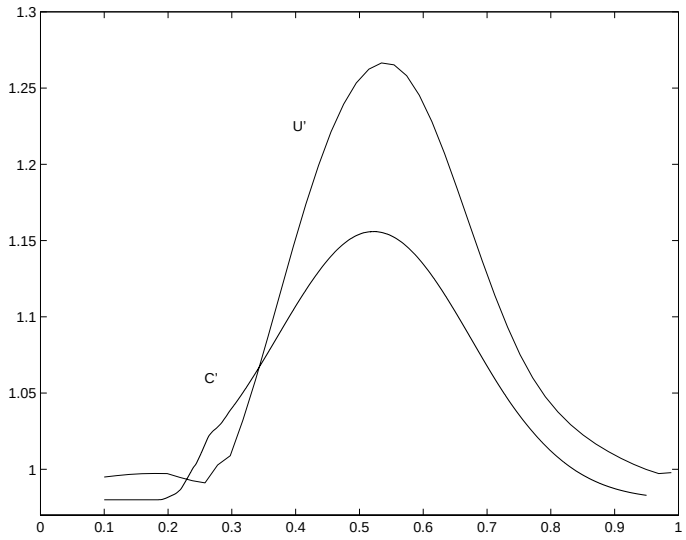

Figure 10: Simulations of the dimensionless underlying, $\mathcal{U}'$, and cyclic, $\mathcal{C}'$, signals for $D = 1$ and $\lambda = 2$.

[4] M. Reading, D. Elliot, and L. Hill, *Some aspects of the theory and practice of modulated differential scanning calorimetry*, in Proceedings of the 21st North American Thermal Analysis Society Conference, Sacramento, CA, 1992, pp. 145–150.

[5] M. Reading, *Modulated differential scanning calorimetry—A new way forward in materials characterization*, Trends Polymer Sci., 1 (1993), pp. 248–253.

[6] M. Reading, A. Luget, and R. Wilson, *Modulated Differential Scanning Calorimetry*, Thermochemica Acta, 238 (1994), pp. 295–307.

[7] M. Reading, R. Wilson, and H. M. Pollock, *Modified differential scanning calorimetry: Theory, practice and applications*, in Proceedings of the 23rd North American Thermal Analysis Society Conference, Toronto, ON, 1994, pp. 2–10.

[8] B. Wunderlich and A. Boller, *Modulated differential scanning calorimetry capabilities and limits*, in Proceedings of the 24th North American Thermal Analysis Society Conference, Sacramento, CA, 1995, pp. 136–141.

[9] B. Wunderlich, A. Boller, I. Okazaki, and S. Kreitmeier, *Linearity, steady state, and complex heat capacity in modulated differential scanning calorimetry*, Thermochim. Acta, 283 (1996), pp. 143–155.

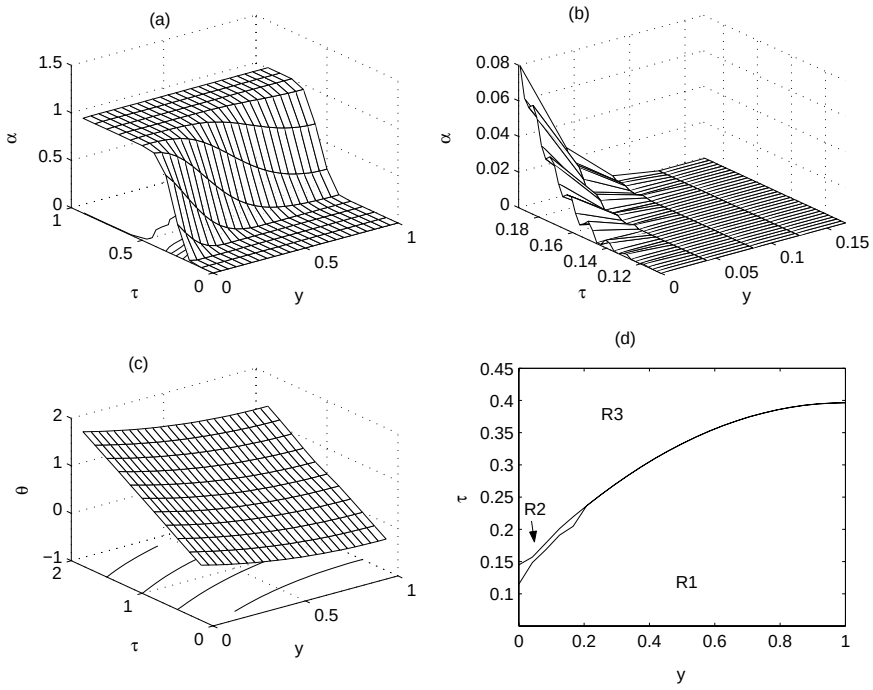

Figure 11: Simulations of the melt fraction α, (a) and (b), dimensionless temperature θ, (c), and the three regimes for $D = 1$ and $\lambda = 0.9$.

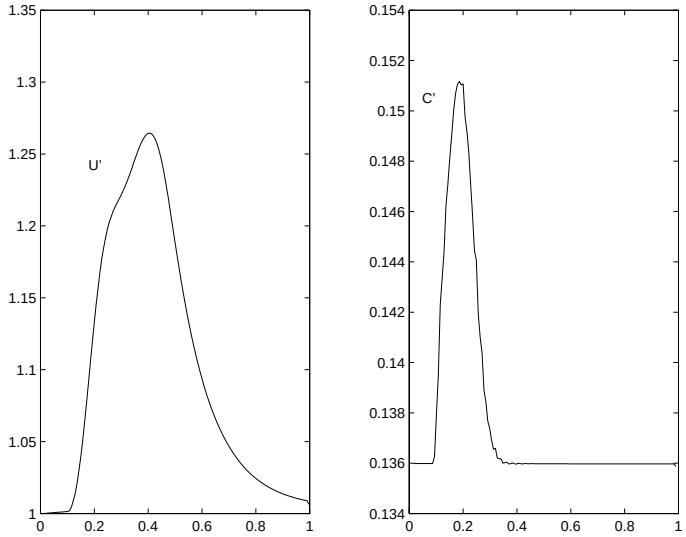

Figure 12: Simulations of the dimensionless underlying, $\mathcal{U}'$, and cyclic, $\mathcal{C}'$, signals for $D = 1$ and $\lambda = 0.9$.